A Kinetic Framework for Modeling Oleochemical Biosynthesis in E. coli

Jackson Peoples[1], Sophia Ruppe[1], Kathryn Mains[1], Elia C. Cipriano[1], and Jerome Fox[1]

[1]University of Colorado Boulder

June 3, 2022

Abstract

Microorganisms build fatty acids with biocatalytic assembly lines, or fatty acid synthases (FASs), that can be repurposed to produce a broad set of fuels and chemicals. Despite their versatility, the product profiles of FAS-based pathways are challenging to adjust without experimental iteration, and off-target products are common. This study uses a detailed kinetic model of the *E. coli* FAS as a foundation to model nine oleochemical pathways. These models provide good fits to experimental data and help explain unexpected results from *in vivo* studies. An analysis of pathways for alkanes and fatty acid ethyl esters, for example, suggests that reductions in titer caused by enzyme overexpression can result from shifts in pools of metabolic intermediates that are incompatible with the substrate specificities of downstream enzymes. In general, different engineering objectives (i.e., production, unsaturated fraction, and average chain length) show experimentally consistent sensitivities to pathway enzymes, and model-based compositional analyses indicate simple shifts in enzyme concentrations can alter the product profiles of pathways with promiscuous components. The study concludes by integrating all models into a graphical user interface. The models supplied by this work provide a versatile kinetic framework for studying oleochemical pathways in different biochemical contexts.

A Kinetic Framework for Modeling Oleochemical Biosynthesis in *E. coli*

Jackson Peoples[a], Sophia Ruppe[a], Kathryn Mains[a], Elia C. Cipriano[a], and Jerome M. Fox[a*]

[a]Department of Chemical and Biological Engineering, University of Colorado, Boulder,

3415 Colorado Avenue, Boulder, CO, 80303

*To whom correspondence should be addressed. E-mail: jerome.fox@colorado.edu

Abstract

Microorganisms build fatty acids with biocatalytic assembly lines, or fatty acid synthases (FASs), that can be repurposed to produce a broad set of fuels and chemicals. Despite their versatility, the product profiles of FAS-based pathways are challenging to adjust without experimental iteration, and off-target products are common. This study uses a detailed kinetic model of the *E. coli* FAS as a foundation to model nine oleochemical pathways. These models provide good fits to experimental data and help explain unexpected results from *in vivo* studies. An analysis of pathways for alkanes and fatty acid ethyl esters, for example, suggests that reductions in titer caused by enzyme overexpression can result from shifts in pools of metabolic intermediates that are incompatible with the substrate specificities of downstream enzymes. In general, different engineering objectives (i.e., production, unsaturated fraction, and average chain length) show experimentally consistent sensitivities to pathway enzymes, and model-based compositional analyses indicate simple shifts in enzyme concentrations can alter the product profiles of pathways with promiscuous components. The study concludes by integrating all models into a graphical user interface. The models

supplied by this work provide a versatile kinetic framework for studying oleochemical pathways in different biochemical contexts.

1 | INTRODUCTION

Microorganisms can produce a diverse set of oleochemicals from renewable feedstocks and are centrally important to the emerging green bioeconomy (Akinsemolu, 2018; Kumar and Kumar, 2017). Microbially produced alcohols, esters, olefines, alkanes, ketones, and polyesters are promising transportation fuels (Bao et al., 2016; Choi and Lee, 2013; Teo et al., 2015), herbicides (Kim et al., 2015), lubricants (Rui et al., 2015), flavors (Lian and Zhao, 2015), fragrances (Goh et al., 2012; Sherkhanov et al., 2016), and polymer additives (Bowen et al., 2016; Clomburg et al., 2015). In engineered microbes, oleochemical biosynthesis typically begins with a fatty acid synthase (FAS), which builds acyl-ACPs of varying lengths, and concludes with the enzymatic conversion of acyl-ACPs to target products ((Sarria et al., 2017; White et al., 2005); Fig. 1). Despite the versatility of FAS-based systems, their activities are challenging to tune—a reflection of their sensitivity to the concentrations, kinetics, and substrate specificities of multiple enzymes (Mains et al., 2022; Ruppe and Fox, 2018; Tan et al., 2018; Xu et al., 2013). This challenge is illustrated by ongoing efforts to engineer oleochemical pathways with well-defined product profiles (Blitzblau et al., 2021; Haushalter et al., 2014; Hernández Lozada et al., 2018; Hernández Lozada et al., 2020); pathway optimization typically requires iteration, and off-target products are common (Grisewood et al., 2017; Sarria et al., 2018).

Mathematical models can facilitate the systematic analysis of cellular metabolism and have guided the design of oleochemical-producing strains. Genome-scale models use the stoichiometries of metabolic networks to predict flux under different growth conditions (Machado and Herrgård, 2015; Zhang and Hua, 2016); when paired with flux balance analysis (FBA), they can reveal genetic adjustments (e.g., gene deletion) likely to re-route flux toward specific products (Agren et al., 2013; Ravi and Gunawan, 2021; Yoshikawa et al., 2017).

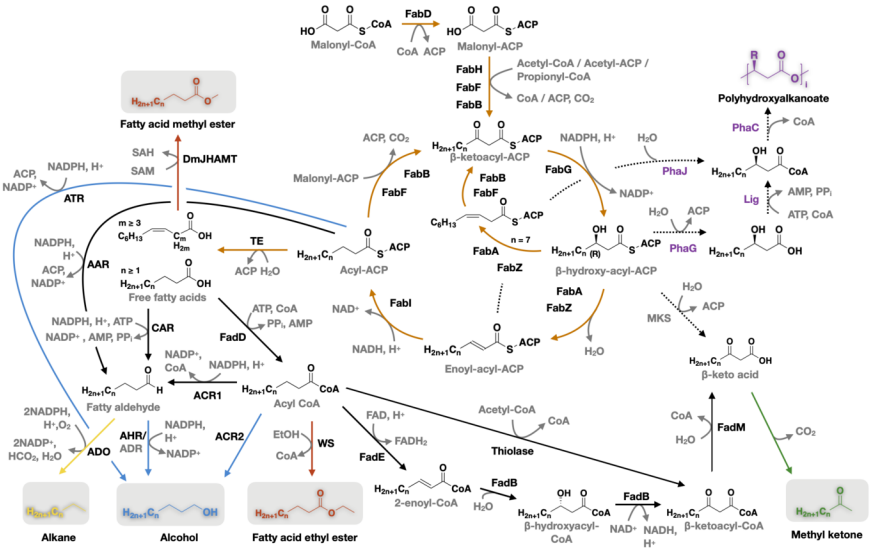

Figure 1. Oleochemical biosynthesis in *E. coli* . The fatty acid synthase (FAS) of*E. coli* (orange) can supply precursors for a broad set of oleochemicals. Engineered pathways tend to exploit either (i) acyl-ACPs, which are important intermediates in fatty acid synthesis, or (ii) free fatty acids, which are released by thioesterase-catalyzed hydrolysis of acyl-ACPs. This study focuses on a subset of oleochemicals (boxes) and enzymatic steps (solid lines). Colors denote enzymatic steps unique to specific products (see Nomenclature for full enzyme names). Pathways not included in this study appear as dotted lines; enzymes that are not included appear in gray.

Unfortunately, these models typically rely on fixed metabolite concentrations and steady-state assumptions

that limit their ability to capture cellular dynamics. Kinetic models derived from reduced genome-scale models can reproduce some dynamic responses to cellular perturbations (e.g., a glucose spike; (van Rosmalen et al., 2021; Stanford et al., 2013)). These models, however, typically lack the resolution required to predict how experimentally relevant changes in the concentrations, kinetics, or substrate specificities of multiple enzymes affect the outputs of complex metabolic processes.

In recent work, we developed a mechanistic kinetic model of the type II FAS of *E. coli* and used it to determine how different FAS components work together to control fatty acid synthesis. Type II FASs, which consist of discrete monofunctional subunits, are common in bacteria and plant plastids. We modeled the *E. coli* FAS as a well-mixed reaction with fixed enzyme concentrations, a constraint supported by the tendency of engineered strains to overproduce free fatty acids in stationary phase (Cho and Cronan, 1995). Our model explained a variety of perplexing results from the literature (e.g., the inhibitory effects of enzyme overexpression) and provided new strategies for engineering FAS systems. Recently, we used it to explore the effects of enzyme concentration on fatty acid synthesis. Using our model alongside *in vitro* and *in vivo* experiments, we showed that simple changes in enzyme concentration can enhance the titers of specific chain lengths by as much as 125-fold (Mains et al., 2022). Our analysis illustrates how kinetic models can guide metabolic engineering.

In this study, we expanded our kinetic model by adding pathways for a diverse set of oleochemicals. These pathways pose a challenge because they include enzymes that are poorly characterized, relative to FAS components. In adding them, we focused on three goals: (i) to develop a framework for incorporating new biosynthetic steps, including those catalyzed by poorly characterized enzymes, (ii) to identify the most influential steps within each pathway, and (iii) to build a graphical user interface (gui) that facilitates model implementation. With these tasks, we sought to build a versatile set of tools for designing oleochemical-producing microbes.

2 | MATERIALS AND METHODS

2.1 | Solution and Optimization of the Kinetic Model

Our models consist of systems of rate equations and mass balances. We solved them by using the MATLAB solver ode15s with relative and absolute error tolerances of 10^{-6} and a vectorization step to reduce solve time. We parameterized the initial model by using parameters reported in experimental studies of purified enzymes or prior modeling analyses, and we adjusted these parameters by using the MATLAB function fminsearch (a derivative-free minimization function) to carry out the fitting routines described below.

We optimized our newly refined model of fatty acid biosynthesis by using a series of objective functions. To incorporate the contributions of FabF and FabZ to unsaturated fatty acid synthesis, we added reactions identical to those used for FabB and FabA, respectively (Tables S1-S2), and we adjusted values of k_{cat} for FabA, FabB, FabZ, and FabF by using Obj_1, where

$Obj_1 = SSE_1$ (Eq. 1)

SSE_1 is the sum of squared errors between measured and predicted unsaturated fractions generated by experimentally reconstituted FASs lacking each enzyme (i.e., we normalized unsaturated fractions by the unsaturated fraction generated by the complete FAS; Tables S3-S4; (Ruppe et al., 2020)). To incorporate the contributions of FabF and FabB to initiation, we used optimization routines that include SSE_2, SSE_3, and SSE_4, the respective sums of squared errors

$Obj_2 = SSE_2 \cdot SSE_3 \cdot SSE_4$ (Eq. 2) $Obj_3 = (1+SSE_2)\cdot(1+SSE_3)\cdot(1+SSE_4)$ (Eq. 3) $Obj_4 = (1+SSE_2)\cdot(1+SSE_3)^2\cdot(1+SSE_4)$ (Eq. 4)

for the time course, product distribution, and initial rates of fatty acid synthesis between modeled and reconstituted FASs. Our optimization process included three steps carried out in series: (i) We removed the production of C_{20} fatty acids, which are not observed experimentally, and used Obj_2 to fit the 18 scaling parameters described in our prior work (Table S5; (Mains et al., 2022)). (ii) Our initial fit caused

an overaccumulation of FabB·acetyl-CoA (Fig. S2). To address this issue, we replaced scaling parameters for the dissociation of FabF·acetyl-ACP and the reversal of FabB activation by acetyl-CoA with parameters that scale FabF binding to malonyl-ACP and FabB binding to acetyl-CoA. We used Obj_3 to optimize these two parameters and two that scale FabF- and FabB-catalyzed decarboxylation of malonyl-ACP (Table S1). (iii) We improved the fit for the product profile by using Obj_4 to fit the same four parameters. Figure S1 shows the results of our optimization. Hereafter, we refer to this model as our "base model". We used it to build the oleochemical-specific models, which used similar optimization routines (SI Methods)

2.2 | Sensitivity analysis

We used the Morris Method to examine the sensitivity of different objectives to various model parameters (e.g., enzyme concentrations or kinetic constants; (Morris, 1991)). This method calculates a set of derivatives (i.e., the change in an objective with respect to a specified parameter) by sampling randomly within a range of parameter values. Briefly, we used the SAFE toolbox with a radial method and Latin hypercube sampling (r = 1,000 trajectories), and verified the convergence of the elementary effects by calculating the first derivative of each parameter's normalized elementary effects with respect to the number of model evaluations (i.e., $|dEE/dn| < 0.0002$) before reporting them (Pianosi et al., 2015). We examined kinetic parameters associated with methyl ketone biosynthesis (Fig. S6) by using parameter ranges of 0.01-100 s^{-1}, and we explored the sensitivity of different biochemical objectives to enzyme concentrations (Fig. 4) by using 0.01-100 μM for all enzymes except those in the alkane pathway; for this low-producing pathway, the narrower range of 1-100 μM enzyme facilitated convergence.

2.3 | Analysis of competing objectives

We constructed "phase diagrams" that depict tradeoffs between average chain length and total production for each alcohol pathway by optimizing enzyme concentrations to maximize or minimize average chain length at different production levels. Briefly, to maximize average chain length, we minimized Obj_5, where L_{norm} is the normalized average chain length (i.e., average

$$Obj_5 = (1\text{-}L_{norm})^2 + (Prod_{target}\text{-}\ Prod)^2 + (Enz_{target}\text{-}\ Enz)^4 \text{ (Eq. 5)}$$

$$Obj_6 = (4/18\text{-}L_{norm})^2 + (Prod_{target}\text{-}\ Prod)^2 + (Enz_{target}\text{-}\ Enz)^4 \text{ (Eq. 6)}$$

chain length divided by 18, the maximum chain length), $Prod_{target}$ is the desired alcohol concentration (palmitic acid equivalents), Prod is the actual alcohol concentration, Enz_{target} is the desired total enzyme concentration, and Enz is the actual enzyme concentration. To minimize average chain length, we minimized Obj_6, where 4/18 is the minimum achievable chain length. For all models, we constrained total enzyme concentration (Enz_{target}) by supplementing the total concentration in our base model with 10 μM of each pathway-specific enzyme: 38 μM for a carboxylic acid reductase (CAR) model, 38 or 48 μM for two acyl-CoA reductase (ACR2 and ACR1) models, and 18 or 108 μM for an acyl-ACP reductase (ATR) model. During each optimization, the concentrations of specific enzymes changed; we retained only results for which differences in both (i) $Prod_{target}$ and Prod and (ii) Enz_{target} and Enz differed by less than 5%.

2.4 | Graphical user interface

We integrated our final models into a graphical user interface (gui) by using MATLAB App Designer. This software package facilitates the design of interactive interfaces with drag-and-drop tools that link to a MATLAB script. We coded the functionality of each added feature (e.g., drop down menus or text boxes) by using the development window, and we adjusted each model slightly to enable integration with the back-end code for the resulting gui.

3 | RESULTS AND DISCUSSION

3.1 | A Refined Model for Fatty Acid Synthesis

In prior work, we developed a detailed kinetic model of the FAS of*E. coli* by modeling the nine enzymes necessary to convert malonyl-CoA and acetyl-CoA to free fatty acids (Fig. 1) (Mains et al., 2022; Ruppe et al.,

2020; Ruppe and Fox, 2018). The model uses rate equations based on detailed reaction mechanisms reported in the literature and includes separate association and dissociation steps for all heteromeric complexes. In this study, we refined our model by incorporating commonly ignored secondary activities of FabZ (β-hydroxyacyl-ACP dehydratase), FabB (β-ketoacyl-ACP synthase I), and FabF (β-ketoacyl-ACP synthase II).

We began by focusing on unsaturated fatty acid synthesis. Previous studies indicate that FabF and FabZ can produce unsaturated fatty acids, although less efficiently than FabA (β-hydroxy-decanoyl-ACP dehydratase) and FabB (Cronan et al., 1969; Feng and Cronan, 2009; Silbert and Vagelos, 1967). We incorporated this set of secondary activities by adding rate equations describing (i) the allylic rearrangement of*trans* -dec-2-enoyl-ACP to *cis* -dec-3-enoyl ACP by FabZ and (ii) the condensation of *cis* -dec-3-enoyl-ACP with malonyl-ACP by FabF. The updated model captured the relative differences in unsaturated fractions between reconstituted FASs lacking FabA, FabB, FabZ, or FabF but underpredicted concentrations of unsaturated products (Tables S3 and S4). This finding is consistent with our observation that *in vitro* systems tend to produce larger unsaturated fractions than*in vivo* systems (Mains et al., 2022; Ruppe et al., 2020), which we used to optimize the original model (and which might reasonably bias the final model toward smaller unsaturated fractions)

Next, we incorporated the contributions of FabF and FabB to acyl chain initiation. Despite their primary role in acyl-ACP elongation, FabF and FabB can also generate β-ketobutyryl-ACP, an intermediate that initiates fatty acid synthesis (i.e., it is the primary product of β-ketoacyl-ACP synthase III, or FabH). To add this activity, we introduced reactions for (i) FabB- and FabF-catalyzed decarboxylation of malonyl-ACP, (ii) FabB-catalyzed condensation of malonyl-ACP with acetyl-ACP or acetyl-CoA to form β-ketobutyryl-ACP, and (iii) FabF- catalyzed condensation of malonyl-ACP with acetyl-ACP to form β-ketobutyryl-ACP (Table S1; (Mains et al., 2022)). We fit this newly expanded model to initial rates and product profiles of experimentally reconstituted FASs (Fig. S1). The final optimized model recreated an unusual C_{18}-rich product profile to which it was not fit (Fig. S3)—an indication that it adequately captures the contributions of different core FAS enzymes to fatty acid synthesis.

3.2 | Biosynthesis of oleochemicals

We expanded our model to include various oleochemicals by adding Michaelis-Menten parameters for new enzymes (SI Methods). These parameters, which are commonly reported in the literature, are reasonable when enzyme-substrate complexes maintain steady-state concentrations during oleochemical production—a reasonable assumption in stationary phase, where protein concentrations are approximately constant, and rates of cell formation and death are approximately equal (Li et al., 2014; Pletnev et al., 2015). With these parameters in hand, we assembled models for the biosynthesis of alcohols, alkanes, methyl ketones, fatty acid methyl esters (FAMEs), and fatty acid ethyl esters (FAEEs) by carrying out two steps: (i) We added estimated values of k_{cat} and K_m for the requisite enzymes (Fig. 1), and (ii) we adjusted enzyme concentrations and kinetic parameters by fitting our model to the product profiles of engineered strains (Figs. 2 and 3). We note: In all fits, we scaled titers reported from experimental cultures to titers expected for *in vitro*systems at 12 minutes (SI Methods). Our models provided good fits to experimental data with two notable exceptions: Tow models for methyl ketone biosynthesis underpredicted the production of either (i) 2-nonanone by a pathway containing *Umbellularia californica*UcFatB1 (BTE), a thioesterase specific for short chains (strain 5 in Fig. 3A), or (ii) palmitic acid by TesA, a thioesterase specific for medium chains that is native to *E. coli* (Fig. 3B). The underprediction of 2-nonanone matches the narrow product profile that we used to parameterize BTE; the associated study may have overlooked minority products. For palmitic acid production by TesA, the large experimental concentration may result from contamination by membrane lipids, which are hydrolyzed in common extraction procedures (Grisewood et al., 2017). Importantly, we recreated the experimental profile by reducing k_{cat} for fatty acid-CoA ligase (FadD) on palmitic acid by four-fold (Fig. S8), but this adjustment is inconsistent with the reported substrate specificity of FadD (i.e., it requires the k_{cat} for C_{16} acyl-CoAs to be lower than for C_{14} and C_{18} substrates (Arora et al., 2005)). In the absence of a strong experimental justification for re-parameterizing the enzymes in question—that is, a rationale for using one experimental dataset over another—we left their kinetic parameters unchanged.

Our modeling analysis allowed us to classify oleochemical pathways by the availability of kinetic data and

the required fitting procedure. We created three groups: (i) Pathways with

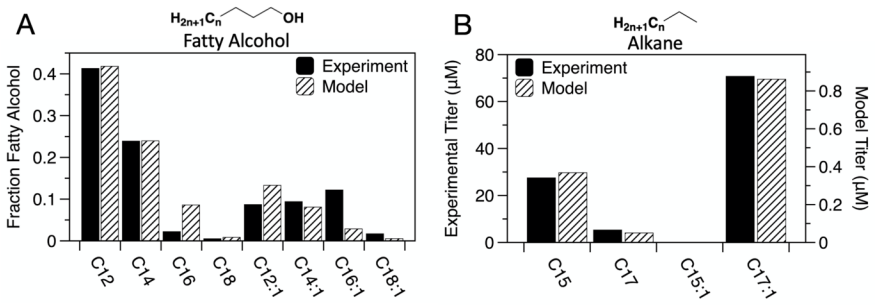

Figure 2. Biosynthesis of fatty alcohols and alkanes. (A) We optimized a model that generates alcohols with a carboxylic acid reductase (CAR) by fitting the product profile of a strain of *E. coli* overexpressing four enzymes: a thioesterase (TE), a CAR, an aldehyde reductase (AHR), and a 4'-phosphopantetheinyl transferase (Sfp; (Kalim Akhtara et al., 2013)). (B) We optimized our model for alkane biosynthesis by fitting the product profile and titer of a strain overexpressing both an acyl-ACP reductase (AAR) and an aldehyde deformylating oxygenase (ADO; (Song et al., 2016)). Table S9 describes the compositions of the modeled pathways.

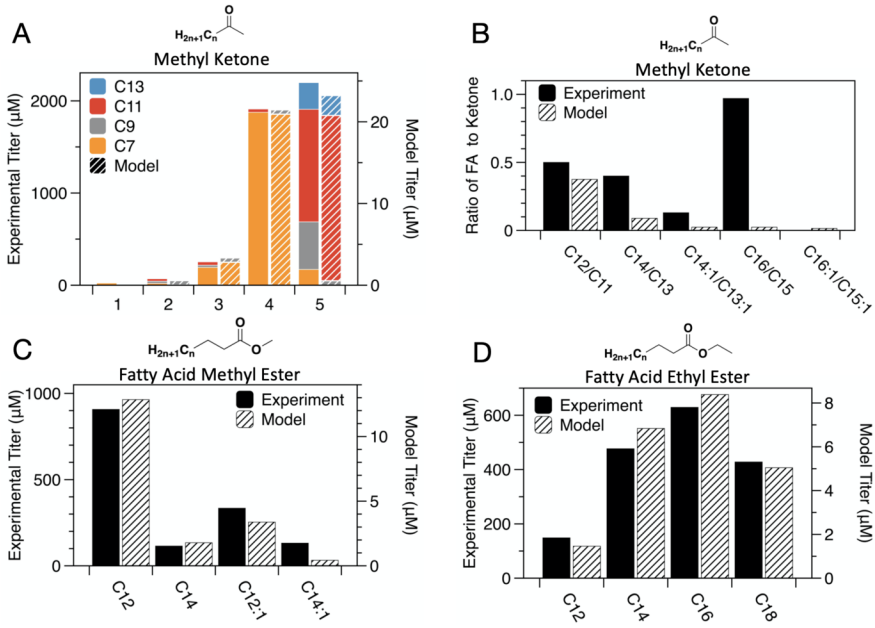

Figure 3. Biosynthesis of methyl ketones and FAEEs. (A-B) We optimized our first set of models for methyl ketone biosynthesis with simultaneous fits to two datasets: (A) the product profiles and titers of five strains that overexpress a thioesterase (TE), a fatty-acid-CoA ligase (FadD), an acyl-CoA dehydrogenase (FadE), an oxidoreductase (FadB), and an acyl-CoA thioesterase (FadM; (Yan et al., 2020)), and (B) the ratio of C_{12} fatty acids to C11 methyl ketones for a sixth strain with similar enzymes overexpressed (Goh et al., 2012). (C-D) We optimized models that generate fatty acid methyl esters (FAMEs) and fatty acid ethyl esters (FAEEs) by fitting the product profiles and titers of strains that overexpress (C) an O-methyltransferase (MT; (Sherkhanov et al., 2016)) or (D) both a wax ester synthase (WS) and a TE, (Steen et al., 2010)). Table S9 describes the compositions of the modeled pathways.

well-characterized enzymes (e.g., an alcohol pathway that uses carboxylic acid reductase, or

CAR, and a thiolase-based methyl ketone pathway discussed later). For these pathways, we fit experimental data by adjusting either a single kinetic parameter or multiple enzyme concentrations (but not both). (ii) Pathways with partially characterized enzymes (e.g., the alkane, FAME, and FAEE pathways). Here, we optimized a single substrate-specific k_{cat} and either (a) multiple enzyme concentrations or (b) an overall k_{cat} vector (i.e., a single factor multiplied by all substrate-specific k_{cat}s). (iii) Pathways with poorly characterized enzymes (e.g., the β-oxidation-based methyl ketone pathway and several alcohol pathways discussed later). Here, we optimized multiple enzyme-specific kinetic parameters. For the methyl ketone pathway, which is poorly characterized, we used a sensitivity analysis to identify the most influential kinetic parameters before fitting. Overall, the reasonable fits afforded by our models indicate that Michaelis-Menten parameters provide an adequate means of modeling the activities of enzymes from different oleochemical pathways (Figs. 2-3).

We parameterized enzymes consistently across models. For each enzyme, we adjusted kinetic parameters only once, and we maintained consistent concentrations between pathways. For example, when optimizing pathway that generates alcohols via a CAR and an aldehyde reductase (AHR), we changed the concentrations of FabA, FabZ, FabB, and FabF—all core FAS enzymes—and retained these concentrations for all models; this constraint is consistent with the native FAS expression levels exploited in most engineered strains. For heterologously expressed enzymes, by contrast, we occasionally adjusted concentrations. TesA, in particular, is common in engineered strains, but its overexpression relies on different promoters and ribosome binding sites (Barrick et al., 1994; Lozano Terol et al., 2021); variability in its concentration between strains is reasonable. In general, the consistent parameterization of enzymes in different pathways suggests that our models can capture the activities of important pathway enzymes in different biochemical contexts.

3.3 | A sensitivity analysis of different models.

Enzyme concentration is an important design consideration for engineered pathways, where it can be controlled with carefully selected promoters, ribosome binding sites, and dynamic transcriptional systems (Meyer et al., 2019; Salis et al., 2009; Zhao et al., 2018). We used a global sensitivity analysis to determine how changes in enzyme concentrations influence three important engineering objectives—the total production, unsaturated fraction, and average length of oleochemical products (Fig. 4). Our results indicate that total production is most sensitive to the concentrations of acyl-ACP thioesterase and downstream oleochemical-specific enzymes, while product profile (i.e., unsaturated fraction and average chain length) is most sensitive to concentrations of acyl-ACP thioesterase and core FAS enzymes. These sensitivities are consistent with the experimentally observed improvements in titer (and constant product profiles) that result from the overexpression of oleochemical-specific enzymes (Song et al., 2016; Yan et al., 2020).

The specific effects revealed by our analysis are consistent with *in vivo* studies. We will briefly comment on a few examples: Starting with the alcohol pathway, we found that concentrations of TesA, CAR, and AHR have a pronounced influence total production, while TesA and FabF affect average chain length. The original study of this pathway did not examine each enzyme in isolation—a difficult feat for an experimental analysis—but it found that the incorporation of a highly active AHR could increase alcohol production (Kalim Akhtara et al., 2013); additionally, shifts in fatty acid compositions produced corresponding shifts in alcohol

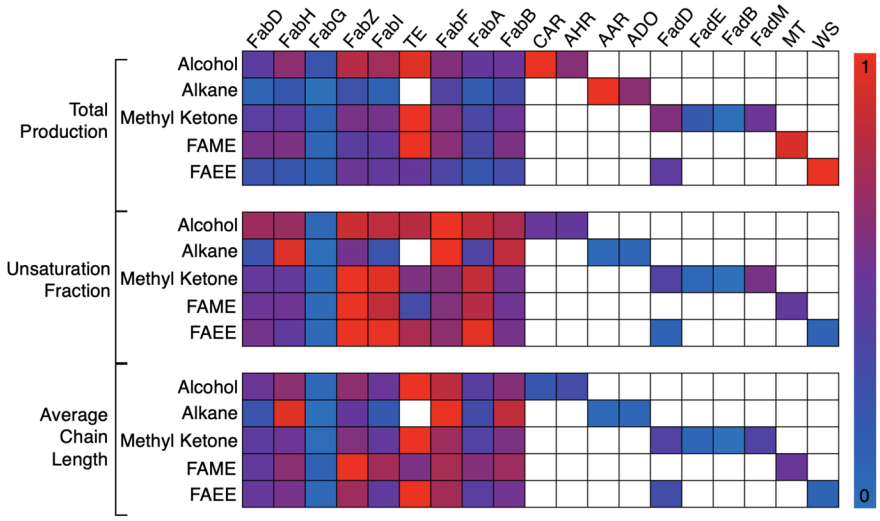

Figure 4 : Sensitivity analyses of oleochemical pathways. We used a global sensitivity analysis to examine the influence of enzyme concentrations on three distinct biochemical objectives: total production, unsaturated fraction, and average length of oleochemical products. In our models, total production is most strongly influenced by the concentrations of either (i) the thioesterase and a single product-specific enzyme or (ii) two product-specific enzymes, while unsaturated fraction and average chain length are most sensitive to the concentrations of core FAS enzymes.

profiles. For the methyl ketone pathway, our results indicate that thioesterase concentration has an outsized influence on both total production and chain length, but also suggest that FadD and β-ketoacyl-CoA thioesterase (FadM) can affect both objectives. This finding is consistent with *in vivo* data showing that the thioesterase, FadD, and FadM need overlapping substrate specificities to maximize the production of specific chain lengths. Importantly, several*in vivo* studies have showed that overexpression of acyl-coenzyme A dehydrogenase (FadE) can improve titers of methyl ketones, but our sensitivity analysis does not reproduce this influence; this discrepancy suggests that FadE may be overactive in our model (Yan et al., 2020). We conclude our brief comparison of general effects by noting that in both model and experiment, the concentrations of final enzymes in the FAME and FAEE pathways (i.e., the O-methyltransferase (MT) and the wax synthase (WS), respectively) strongly influence total production, perhaps a result of their low activities, relative to other enzymes (Sherkhanov et al., 2016; Steen et al., 2010).

We used our models to investigate several intriguing effects from*in vivo* studies. An experimental study of the alkane pathway examined different expression levels of acyl-ACP reductase (AAR) and (ii) an aldehyde deformylating oxygenase (ADO) by using alternative plasmids, promoters, and pseudo-operon configurations (Song et al., 2016). Shifts in the expression of both enzymes had a prominent influence on total production, but not product profile. We recreated this effect by changing the AAR:ADO ratio in our model; production peaked at an intermediate ratio, while average chain length stayed constant (Figs. 5A-5B). This behavior suggests that AAR and ADO catalyze rate-limiting steps and must be overexpressed at similar levels to improve titer. Their inability to affect product profile, in turn, probably reflects their narrow substrate specificities (i.e., C_{16} and C_{18}). Intriguingly, the same experimental study also showed that the overexpression of FabH and FabB can reduce alkane production. Our model

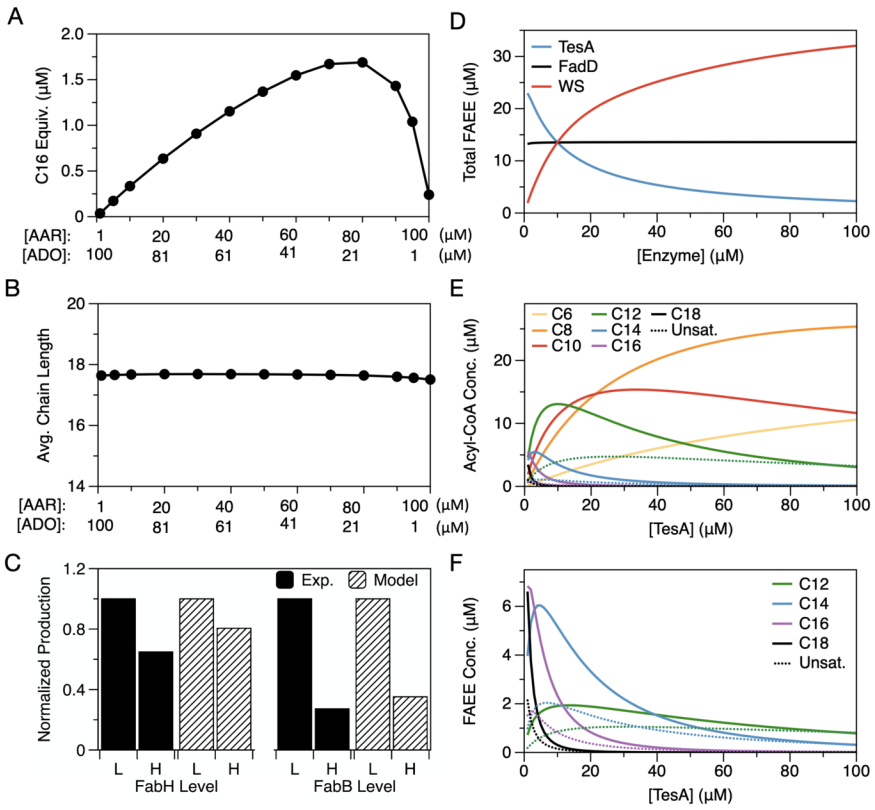

Figure 5 . Concentration effects in alkane and FAEE pathways. The FAS supplemented with (A-C) an acyl-ACP reductase (AAR) and an aldehyde deformylating oxygenase (ADO) or (D-F) an acyl-ACP thioesterase specific for medium chains (TesA), a fatty-acid-CoA ligase (FadD), and a wax synthase (WS). (A) Alkane production peaks at a high AAR:ADO ratio, which does not alter (B) average chain length. (C) Overexpression of β-ketoacyl-ACP synthase III (FabH) or β-ketoacyl-ACP synthase I (FabB) decrease alkane production *in vivo* (black) and in our model (i.e., 1 μM to 100 μM; white with black hatching). (D) Increasing concentrations of WS increase FAEE production, while TesA decreases it; FadD has no effect. (E) High concentrations of TesA increase the production of short-chain acyl-CoAs at the expense of long-chain acyl-CoAs, the preferred substrates of WS. (F) FAEE production decreases as a result. In A-F, the concentrations of pathway enzymes not mentioned are unchanged from Figs. 2B and 3B.

recreates this effect and suggests that it results from a reduction in appropriately sized acyl-ACPs (Fig. 5C). In brief, FabH overexpression increases short-chain acyl-ACPs, at the expense of long chains, while FabB overexpression sequesters long-chain acyl-ACPs in FabBwACP complexes (Fig. S10). Both effects reduce the pool of substrates for AAR.

Next, we turned to the FAEE pathway. In an early study of this pathway, TesA overexpression reduced FAEE titers (Steen et al., 2010). We speculated that this effect, which is recreated in our model (Fig. 5D), might result from a mismatch between (i) the pool of available acyl-ACPs and (ii) the substrate specificity of WS. Our model allowed us to explore this mismatch. As expected, high concentrations of TesA increased the production of short-chain acyl-ACPs at the expense of long chains, which are the preferred substrates of WS (Figs. 5E-5F). Our focused analyses of alkane and FAEE production illustrates the importance of kinetic models that capture changes in concentrations of length-specific metabolic intermediates.

3.4 | A comparison of competing objectives in alternative alcohol pathways.

Our prior work on fatty acid biosynthesis indicates that coordinated shifts in enzyme concentration can tune

average chain length—a critical design objective of engineered systems—without altering total production (Mains et al., 2022). We sought to evaluate this engineering strategy in four pathways for alcohol biosynthesis, where control over length remains difficult. We began by supplementing our first alcohol pathway, which relies on FadD, a CAR, and an aldehyde reductases (AHR), with three additional pathways that extend the core FAS with 1-4 enzymes: (i) an acyl-ACP reductase (ATR), (ii) a TesA, FadD, and an acyl-CoA reductase (ACR2), or (iii) TesA, FadD, a different acyl-CoA reductase (ACR1), and an aldehyde reductase (AHR). As before, we added new enzymes to our base model and optimized poorly characterized kinetic parameters with fits to experimental data (Fig. S5). With our four alternative models in hand, we examined the range of average chain lengths accessible with simple shifts in enzyme concentration. Intriguingly, for all pathways, the breadth of chain lengths decreases as total production increases, and the highest production levels culminate in a single average chain length (Fig. 6). This tradeoff is sharpest for the ATR and ACR1 pathways (Figs. 6B and 6D), where critical enzymes—namely ATR and ACR1—have very narrow substrate specificities. The CAR and ACR2 pathways, by contrast, enable broad control until very high production levels, with the CAR pathway providing the greatest flexibility (Fig. 6A and 6C). The control afforded by this pathway reflects the broad substrate specificities of all enzymes downstream of the FAS.

An analysis of enzyme compositions at high and low average chain lengths reveals the mechanisms of control (Dataset S1). For the CAR, ACR1, and ACR2 pathways, high concentrations of TesA and low concentrations of FabF and FabB facilitate the production of short-chain alcohols, while the opposite shifts encourage long-chain products. This trend is consistent with influence of TesA, FabF, and FabB on fatty acid biosynthesis (Mains et al., 2022). Results also suggest that a reduction in FabA concentration and increase in FabZ can promote the production of short-chain alcohols—perhaps, the result of the preference of FabZ for short substrates—but this effect is less pronounced (i.e., changes in enzyme concentrations are smaller than those of TesA, FabF, and FabB). For the ATR pathway, which has no thioesterase, chain length appeared most sensitive to the concentrations of FabB and FabA (with trends consistent with those exhibited by the other pathways).

For each pathway, we used a total enzyme concentration informed by the overexpression strategy described in an experimental study. The ATR and ACR1 enzymes, however, are not particularly active, and high enzyme concentrations could blunt the tradeoff between chain

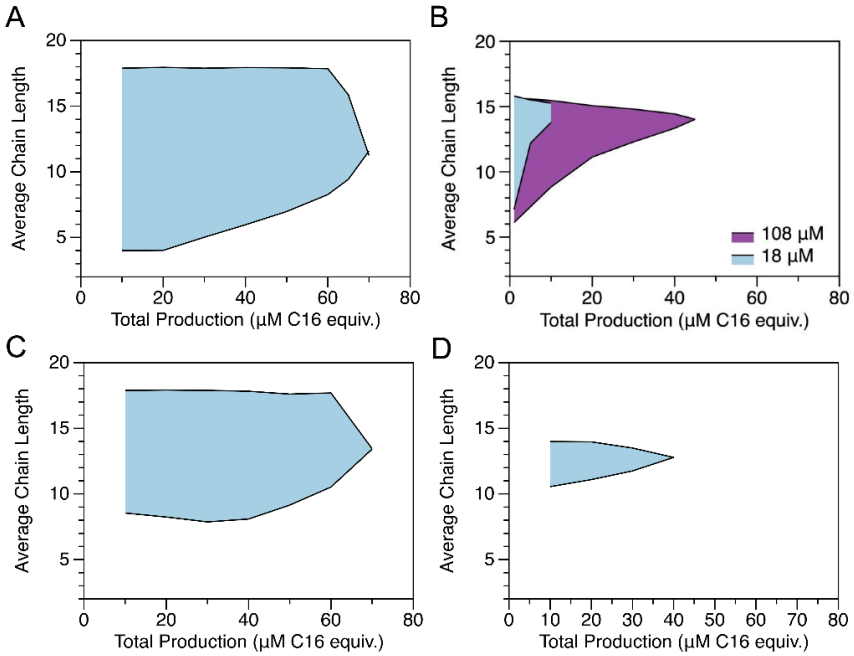

Figure 6. A comparison of different pathways for alcohol biosynthesis. (A-D) The range of average chain lengths afforded by alternative alcohol pathways: FAS supplemented with (A) TesA, CAR, and AHR, (B) acyl-ACP reductase (ATR), (C) acyl-ACP thioesterase specific for medium chains (TesA), a fatty-acid-CoA ligase (FadD), and an acyl-CoA reductase (ACR2), and (D) TesA, FadD, a differentacyl-CoA reductase (ACR1), and an aldehyde reductase (AHR). At each production level, the shaded region denotes the average chain lengths achievable by changing enzyme concentrations; the range of lengths narrows as production increases. Dataset S1 contains the source data and enzyme compositions for plots A-D.

length and production. We explored this effect by repeating the ATR analysis with a much higher enzyme concentration (˜ninefold). This adjustment broadened the range of accessible chain lengths at intermediate production levels. We note, however, that our model does not account for the potential for ATR to bind holo-ACP, an interaction that can inhibit fatty acid synthesis and may limit the usefulness of ATR overexpression.

A sensitivity analysis of all pathways examined in this work suggests that, in general, product profiles are most sensitive to concentrations of acyl-ACP thioesterases and β-ketoacyl-ACP synthases (Fig. S11). This sensitivity, however, does not imply that all pathways are compatible with concentration-based control strategies; the narrow substrate specificities of ATR and ACR1, for example, are limiting. Rather, our focused analysis of the alcohol pathways suggest that coordinated changes in enzyme concentration provide a versatile means of tuning the product profiles of pathways with promiscuous enzymes downstream of the FAS.

3.5 | A graphical user interface for modeling oleochemical biosynthesis

To facilitate the rapid implementation of our models, we integrated them into a MATLAB-based graphical user interface (gui; Fig. 7). This gui permits user-defined changes in enzyme, substrate, and cofactor concentrations, and allows the user to specify alternative versions of enzymes explored in this study (e.g., different thioesterases). Its plotting feature can generate final product profiles at user-defined time points or time courses for specific metabolites (e.g., acyl-ACPs). Motivated by our analysis of different alcohol pathways, we added a thiolase-based pathway for methyl ketone production (Fig. S9). The final gui includes nine pathways, each parameterized with a mixture of*in vitro* and *in vivo* studies.

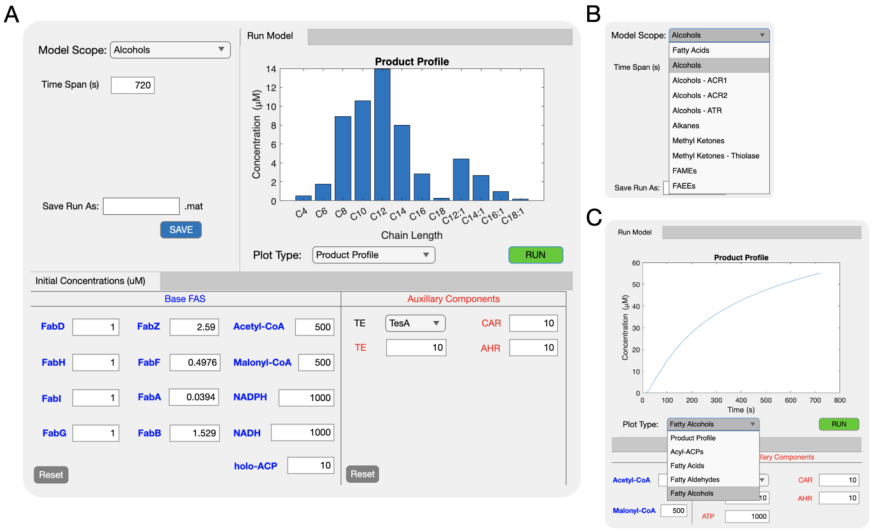

Figure 7 . A graphical user interface. (A) A MATLAB-compatible graphical user interface (gui) facilitates modeling analyses of different (B) oleochemical pathways and (C) metabolites. Note: The 12-minute time point provides a convenient means of exploring the influence of enzyme compositions on final product profiles; we used this time point in the analyses of Figs. 2-6.

4 | CONCLUSION

Oleochemical-producing microbes with arbitrary, user-defined product profiles remain an elusive goal of metabolic engineering (Marella et al., 2018; Sharma and Yazdani, 2021; Yan and Pfleger, 2019). The activities and substrate specificities of critical enzymes are difficult to predict (or change), and their integration into new pathways typically requires multiple rounds of iteration; titer and product profile, in particular, tend to be nonintuitively coupled (Greenhalgh et al., 2021; Grisewood et al., 2017; Sarria et al., 2018). In this study, we developed a set of kinetic models that facilitates the design and analysis of oleochemical pathways. These models provide good fits to experimental data and can capture the effects of previously reported pathway modifications. The final models enable mechanistic studies of unexpected phenomena (e.g., the inhibition of FAEE biosynthesis by TesA overexpression) and facilitate large, system-wide analyses that are experimentally intractable. Our sensitivity analysis, for example, allowed us to probe the influence of isolated shifts in protein concentration within a broad set of pathways. Findings indicate that product profiles are most sensitive to concentrations of FabB, FabF, and acyl-ACP thioesterase (when present) and indicate that coordinated shifts in these concentrations can adjust the product profiles of pathways with promiscuous enzymes downstream of the FAS. Oleochemical-specific enzymes, in turn, primarily influence total production, an indication that their overexpression can improve titer without altering final product profiles. These observations provide guidance for optimizing enzyme expression levels in oleochemical pathways.

The incorporation of different oleochemical pathways into our FAS model allowed us to refine general rules for characterizing pathway enzymes. Results indicate that substrate-specific Michaelis-Menten parameters are sufficient to capture the activities of a broad set of enzymes. These parameters rely on steady-state assumptions that are reasonable during oleochemical production in stationary phase. Importantly, our consistent parameterization of enzymes between pathways suggests that our models can capture their activities in different biochemical contexts. Enzyme-specific kinetic parameters are most accurately measured with *in vitro* kinetic assays (e.g., the CAR-based alcohol pathway), but our results indicate that *in vivo* product profiles that differ in the identity or expression level of individual enzymes can also support reasonable estimates (e.g., alternative thioesterases). Finally, protein expression levels, which can vary between strains (Monk et al., 2016), are important for accurate and consistent kinetic models. The regular use of proteomics to measure protein concentrations in engineered strains could improve model accuracy and help explain strain-to-strain variability in oleochemical pathways.

The paper concludes by developing a gui to facilitate the rapid implementation of our models. This gui is a useful tool for exploring the influence of various pathway modifications on final product profiles and could guide experimental studies (e.g., promoter selection or configuration). It complements the complete model files, which enable detailed analyses of oleochemical production (e.g., plots of various metabolites or analyses of tradeoffs between objectives) with minor changes in code or short optimization routines. Together, the gui and its core models provide a versatile kinetic framework for studying oleochemical biosynthesis.

ACKNOWLEDGEMENTS

This work was supported by the United States Army Research Office (J.P., S.R., K.M. E.C.P., and J.M.F., award W911NF-18-1-0159). J.P. acknowledges support from the National Science Foundation (J.P., award 1804897) for a summer research experience that supported his initial work on this project. K.M. acknowledges fellowship support from the Department of Defense (DoD) through the National Defense Science & Engineering Graduate (NDSEG). E.C.C. acknowledges fellowship support from the NIH/CU Molecular Biophysics Program and NIH Biophysics Training Grant T32 GM-065103.

DATA AVAILABILITY STATEMENT

Code associated with this work is available online at https://github.com/jmfoxai/versatilemodel1. All other data is available from the corresponding author upon reasonable request.

SUPPORTING INFORMATION

Additional supporting information may be found in the online version of the article at the publisher's website.

ORCID

Jackson Peoples: https://orcid.org/0000-0003-3261-582X

Sophia Ruppe: https://orcid.org/0000-0003-0743-8796

Kathryn Mains: https://orcid.org/0000-0002-3623-1383

Elia C. Cipriano: https://orcid.org/0000-0001-5460-4094

Jerome M. Fox: https://orcid.org/0000-0002-3739-1899

NOMENCLATURE

FAS, fatty acid synthase; FAME, fatty acid methyl ester; FAEE, fatty acid ethyl ester; ACP, acyl carrier protein; CoA, coenzyme-A; FabD, Malonyl CoA-ACP transacylase; CO_2, carbon dioxide; NADPH, reduced nicotinamide adenine dinucleotide phosphate; H^+, hydrogen ion; $NADP^+$, nicotinamide adenine dinucleotide phosphate; FabA, β-hydroxy-decanoyl-ACP dehydratase; FabZ, β-hydroxyacyl-ACP dehydratase; NADH, reduced nicotinamide adenine dinucleotide; NAD^+, nicotinamide adenine dinucleotide; FabI, enoyl-ACP reductase; FabF, β-ketoacyl-ACP synthase II; FabB, β-ketoacyl-ACP synthase I; FabH; β-ketoacyl-ACP synthase III; TE, thioesterase; TesA, thioesterase I; H_2O, water; SAM, S-adenosyl-L-methionine; SAH, S-adenosyl-L-homocysteine; DmJHAMT or MT, *Drosophila melanogaster*juvenile hormone acid O-methyltransferase; ATP, adenosine triphosphate; AMP, adenosine monophosphate; ADP, adenosine diphosphate; P_i, phosphate; PP_i, pyrophosphate; CAR, carboxylic acid reductase; ACR, acyl-ACP/acyl-CoA reductase; ATR, acyl-ACP reductase; ADH, alcohol dehydrogenase; AHR, aldehyde reductase; ADO, aldehyde deformylating oxygenase; O_2, oxygen; FadD, fatty acid-CoA ligase; WS, wax ester synthase; EtOH, ethanol; FadE, acyl-CoA dehydrogenase; FAD, flavin adenine dinucleotide; $FADH_2$, reduced flavin adenine dinucleotide; FadB, 3-hydroxyacyl-CoA dehydrogenase; FadM, β-ketoacyl-CoA thioesterase; MKS, methyl ketone synthase; PhaG, (R)-3-hydroxydecanoyl-ACP:CoA transacylase; FabG, β-ketoacyl-ACP reductase; PhaJ, (R)-enoyl-CoA hydratase; Lig, ligase; PhaC, PHA synthase; PHA, polyhydroxyalkanoate; FadA, 3-keto-acyl-CoA thiolase.

References

Agren R, Otero JM, Nielsen J. 2013. Genome-scale modeling enables metabolic engineering of Saccharomyces cerevisiae for succinic acid production. *J. Ind. Microbiol. Biotechnol.* **40** :735–747.

Akinsemolu AA. 2018. The role of microorganisms in achieving the sustainable development goals. *J. Clean. Prod.***182** :139–155.

Arora P, Vats A, Saxena P, Mohanty D, Gokhale RS. 2005. Promiscuous Fatty Acyl CoA Ligases Produce Acyl-CoA and Acyl-SNAC Precursors for Polyketide Biosynthesis. *J. Am. Chem. Soc.***127** :9388–9389. https://doi.org/10.1021/ja052991s.

Bao L, Li JJ, Jia C, Li M, Lu X. 2016. Structure-oriented substrate specificity engineering of aldehyde-deformylating oxygenase towards aldehydes carbon chain length. *Biotechnol. Biofuels***9** :1–14.

Barrick D, Villanueba K, Childs J, Kalil R, Schneider TD, Lawrence CE, Gold L, Stormo GD. 1994. Quantitative analysis of ribosome binding sites in E.coli. *Nucleic Acids Res.* **22** :1287–1295.

Blitzblau HG, Consiglio AL, Teixeira P, Crabtree D V., Chen S, Konzock O, Chifamba G, Su A, Kamineni A, MacEwen K, Hamilton M, Tsakraklides V, Nielsen J, Siewers V, Shaw AJ. 2021. Production of 10-methyl branched fatty acids in yeast. *Biotechnol. Biofuels* **14** :1–17.

Bowen CH, Bonin J, Kogler A, Barba-Ostria C, Zhang F. 2016. Engineering Escherichia coli for Conversion of Glucose to Medium-Chain ω-Hydroxy Fatty Acids and α,ω-Dicarboxylic Acids. *ACS Synth. Biol.***5** :200–206.

Cho H, Cronan JE. 1995. Defective export of a periplasmic enzyme disrupts regulation of fatty acid synthesis. *J. Biol. Chem.*

Choi YJ, Lee SY. 2013. Microbial production of short-chain alkanes.*Nature* **502** :571–4. http://www.ncbi.nlm.nih.gov/pubmed/24077097.

Clomburg JM, Blankschien MD, Vick JE, Chou A, Kim S, Gonzalez R. 2015. Integrated engineering of β-oxidation reversal and ω-oxidation pathways for the synthesis of medium chain ω-functionalized carboxylic acids.*Metab. Eng.* **28** :202–212.

Cronan JE, Birge CH, Vagelos PR. 1969. Evidence for two genes specifically involved in unsaturated fatty acid biosynthesis in Escherichia coli. *J. Bacteriol.*

Feng Y, Cronan JE. 2009. Escherichia coli unsaturated fatty acid synthesis. Complex trancription of the fabA gene and in vivo identification of the essential reaction catalyzed by FabB. *J. Biol. Chem.* **284** :29526–35.

Goh EB, Baidoo EEK, Keasling JD, Beller HR. 2012. Engineering of bacterial methyl ketone synthesis for biofuels. *Appl. Environ. Microbiol.* **78** :70–80.

Greenhalgh JC, Fahlberg SA, Pfleger BF, Romero PA. 2021. Machine learning-guided acyl-ACP reductase engineering for improved in vivo fatty alcohol production. *Nat. Commun.* **12** :5825. https://doi.org/10.1038/s41467-021-25831-w.

Grisewood MJJ, Hernández-Lozada NJJ, Thoden JBB, Gifford NPP, Mendez-Perez D, Schoenberger HAA, Allan MFF, Floy MEE, Lai R-YY, Holden HMM, Pfleger BFF, Maranas CDD. 2017. Computational Redesign of Acyl-ACP Thioesterase with Improved Selectivity toward Medium-Chain-Length Fatty Acids. *ACS Catal.* **7** :3837–3849.

Haushalter RW, Kim W, Chavkin TA, The L, Garber ME, Nhan M, Adams PD, Petzold CJ, Katz L, Keasling JD. 2014. Production of anteiso-branched fatty acids in Escherichia coli; next generation biofuels with improved cold-flow properties. *Metab. Eng.* **26** :111–118.

Hernández Lozada NJ, Simmons TR, Xu K, Jindra MA, Pfleger BF. 2020. Production of 1-octanol in Escherichia coli by a high flux thioesterase route. *Metab. Eng.* **61** :352–359.

Hernández Lozada NJ, Lai R-Y, Simmons TR, Thomas KA, Chowdhury R, Maranas CD, Pfleger BF. 2018. Highly Active C8-Acyl-ACP Thioesterase Variant Isolated by a Synthetic Selection Strategy. *ACS Synth. Biol.* **7** :2205–2215.

Kalim Akhtara M, Turner NJ, Jones PR. 2013. Carboxylic acid reductase is a versatile enzyme for the conversion of fatty acids into fuels and chemical commodities. *Proc. Natl. Acad. Sci. U. S. A.***110** :87–92.

Kim S, Clomburg JM, Gonzalez R. 2015. Synthesis of medium-chain length (C6–C10) fuels and chemicals via β-oxidation reversal in Escherichia coli. *J. Ind. Microbiol. Biotechnol.* **42** :465–475.

Kumar R, Kumar P. 2017. Future microbial applications for bioenergy production: A perspective. *Front. Microbiol.* **8** :1–4.

Li Z, Nimtz M, Rinas U. 2014. The metabolic potential of Escherichia coli BL21 in defined and rich medium. *Microb. Cell Fact.***13** :1–17.

Lian J, Zhao H. 2015. Reversal of the β-oxidation cycle in saccharomyces cerevisiae for production of fuels and chemicals. *ACS Synth. Biol.* **4** :332–341.

Lozano Terol G, Gallego-Jara J, Sola Martínez RA, Martínez Vivancos A, Cánovas Díaz M, de Diego Puente T. 2021. Impact of the Expression System on Recombinant Protein Production in Escherichia coli BL21. *Front. Microbiol.* **12** :1–12.

Machado D, Herrgård MJ. 2015. Co-evolution of strain design methods based on flux balance and elementary mode analysis. *Metab. Eng. Commun.* **2** :85–92.

Mains K, Peoples J, Fox JM. 2022. Kinetically guided, ratiometric tuning of fatty acid biosynthesis. *Metab. Eng.* **69** :209–220.

Marella ER, Holkenbrink C, Siewers V, Borodina I. 2018. Engineering microbial fatty acid metabolism for biofuels and biochemicals.*Curr. Opin. Biotechnol.* **50** :39–46.

Meyer AJ, Segall-Shapiro TH, Glassey E, Zhang J, Voigt CA. 2019. Escherichia coli "Marionette" strains with 12 highly optimized small-molecule sensors. *Nat. Chem. Biol.*

Monk JM, Koza A, Campodonico M, Machado D, Seoane JM, Palsson BO, Herrgård MJ, Feist AM. 2016. Multi-omics quantification of species variation of Escherichia coli links molecular features with strain phenotypes. *Cell Syst.* **3** :238–251.

Morris MD. 1991. Factorial sampling plans for preliminary computational experiments. *Technometrics* **33** :161–174.

Pianosi F, Sarrazin F, Wagener T. 2015. A Matlab toolbox for Global Sensitivity Analysis. *Environ. Model. Softw.* **70** :80–85.

Pletnev P, Osterman I, Sergiev P, Bogdanov A, Dontsova O. 2015. Survival guide: Escherichia coli in the stationary phase. *Acta Naturae***7** :22–33.

Ravi S, Gunawan R. 2021. ΔFBA-Predicting metabolic flux alterations using genome-scale metabolic models and differential transcriptomic data. *PLoS Comput. Biol.* **17** :1–18.

van Rosmalen RP, Smith RW, Martins dos Santos VAP, Fleck C, Suarez-Diez M. 2021. Model reduction of genome-scale metabolic models as a basis for targeted kinetic models. *Metab. Eng.* **64** :74–84.

Rui Z, Harris NC, Zhu X, Huang W, Zhang W. 2015. Discovery of a Family of Desaturase-Like Enzymes for 1-Alkene Biosynthesis. *ACS Catal.***5** :7091–7094.

Ruppe A, Fox JM. 2018. Analysis of Interdependent Kinetic Controls of Fatty Acid Synthases. *ACS Catal.* **8** :11722–11734.

Ruppe A, Mains K, Fox JM. 2020. A kinetic rationale for functional redundancy in fatty acid biosynthesis. *Proc. Natl. Acad. Sci.* :202013924.

Salis HM, Mirsky EA, Voigt CA. 2009. Automated design of synthetic ribosome binding sites to control protein expression. *Nat. Biotechnol.* **27** :946–950.

Sarria S, Bartholow TG, Verga A, Burkart MD, Peralta-Yahya P. 2018. Matching Protein Interfaces for Improved Medium-Chain Fatty Acid Production. *ACS Synth. Biol.* **7** :1179–1187.

Sarria S, Kruyer NS, Peralta-Yahya P. 2017. Microbial synthesis of medium-chain chemicals from renewables. *Nat. Biotechnol.***35** :1158–1166.

Sharma A, Yazdani SS. 2021. Microbial engineering to produce fatty alcohols and alkanes. *J. Ind. Microbiol. Biotechnol.* **48** .

Sherkhanov S, Korman TP, Clarke SG, Bowie JU. 2016. Production of FAME biodiesel in E. coli by direct methylation with an insect enzyme.*Sci. Rep.* **6** :1–10.

Silbert DF, Vagelos PR. 1967. Fatty acid mutant of E. coli lacking a beta-hydroxydecanoyl thioester dehydrase. *Proc. Natl. Acad. Sci. U. S. A.* **58** :1579–1586.

Song X, Yu H, Zhu K. 2016. Improving alkane synthesis in Escherichia coli via metabolic engineering. *Appl. Microbiol. Biotechnol.***100** :757–767.

Stanford NJ, Lubitz T, Smallbone K, Klipp E, Mendes P, Liebermeister W. 2013. Systematic construction of kinetic models from genome-scale metabolic networks. *PLoS One* **8** .

Steen EJ, Kang Y, Bokinsky G, Hu Z, Schirmer A, McClure A, Del Cardayre SB, Keasling JD. 2010. Microbial production of fatty-acid-derived fuels and chemicals from plant biomass. *Nature* **463** :559–562. http://dx.doi.org/10.1038/nature08721.

Tan Z, Yoon JM, Chowdhury A, Burdick K, Jarboe LR, Maranas CD, Shanks J V. 2018. Engineering of E. coli inherent fatty acid biosynthesis capacity to increase octanoic acid production. *Biotechnol. Biofuels* **11** :1–15.

Teo WS, Ling H, Yu AQ, Chang MW. 2015. Metabolic engineering of Saccharomyces cerevisiae for production of fatty acid short- and branched-chain alkyl esters biodiesel. *Biotechnol. Biofuels***8** :1–9.

White SW, Zheng J, Zhang Y-M, Rock, Rock CO, Rock. 2005. The structural biology of type II fatty acid biosynthesis. *Annu. Rev. Biochem.***74** :791–831.

Xu P, Gu Q, Wang W, Wong L, Bower AGW, Collins CH, Koffas MAG. 2013. Modular optimization of multi-gene pathways for fatty acids production in E. coli. *Nat. Commun.* **4** :1408–1409.

Yan Q, Pfleger BF. 2019. Revisiting metabolic engineering strategies for microbial synthesis of oleochemicals. *Metab. Eng.***58** :35–46.

Yan Q, Simmons TR, Cordell WT, Hernández Lozada NJ, Breckner CJ, Chen X, Jindra MA, Pfleger BF. 2020. Metabolic engineering of β-oxidation to leverage thioesterases for production of 2-heptanone, 2-nonanone and 2-undecanone. *Metab. Eng.* **61** :335–343.

Yoshikawa K, Toya Y, Shimizu H. 2017. Metabolic engineering of Synechocystis sp. PCC 6803 for enhanced ethanol production based on flux balance analysis. *Bioprocess Biosyst. Eng.* **40** :791–796.

Zhang C, Hua Q. 2016. Applications of genome-scale metabolic models in biotechnology and systems medicine. *Front. Physiol.***6** :1–8.

Zhao EM, Zhang Y, Mehl J, Park H, Lalwani MA, Toettcher JE, Avalos JL. 2018. Optogenetic regulation of engineered cellular metabolism for microbial chemical production. *Nature* **555** :683–687.